

RESEARCH PAPER

 OPEN ACCESS 

HuR stabilizes *HTT* mRNA via interacting with its exon 11 in a mutant *HTT*-dependent manner

Quan Zhao^a, Chen Li^a, Meng Yu^a, Yimin Sun^a, Jian Wang ^a, Lixiang Ma^b, Xiaoli Sun^{a,c}, and Boxun Lu ^a

^aNeurology Department at Huashan Hospital, State Key Laboratory of Medical Neurobiology and MOE Frontiers Center for Brain Science, Institutes of Biomedical Sciences, School of Life Sciences, Fudan University, Shanghai, China; ^bDepartment of Anatomy, Histology and Embryology, Shanghai Basic Medical College, Fudan University, Shanghai, China; ^cShanghai Xuhui District Central Hospital, Zhongshan Xuhui Hospital, Fudan University, Shanghai, China

ABSTRACT

Huntington's Disease (HD) is a monogenetic neurodegenerative disorder mainly caused by the cytotoxicity of the mutant *HTT* protein (mHTT) encoded by the mutant *HTT* gene. Lowering *HTT* mRNA has been extensively studied as a potential therapeutic strategy, but how its level is regulated endogenously has been unclear. Here we report that the RNA-binding protein (RBP) HuR interacts with and stabilizes *HTT* mRNA in an mHTT-dependent manner. In HD cells but not wild-type cells, siRNA knockdown or CRISPR-induced heterozygous knockout of HuR decreased *HTT* mRNA stability. HuR interacted with *HTT* mRNA at a conserved site in exon 11 rather than the 3'-UTR region of the mRNA. Interestingly, this interaction was dependent on the presence of mHTT, likely *via* the activation of MAPK11, which enhanced cytosolic localization of the HuR protein. Thus, mHTT, MAPK11 and HuR may form a positive feedback loop that stabilizes *HTT* mRNA and enhances mHTT accumulation, which may contribute to HD progression. Our data reveal a novel regulatory mechanism of *HTT* mRNA *via* non-canonical binding of HuR.

ARTICLE HISTORY

Received 5 September 2019
Revised 27 December 2019
Accepted 30 December 2019

KEYWORDS

RNA binding protein; CAG repeats; polyglutamine; Huntington's disease; MAPK11; p38; neurodegeneration

Introduction

Huntington's disease (HD) is an important monogenetic neurodegenerative disorder mainly caused by the mutation of the *HTT* gene [1], which encodes the mutant *HTT* protein (mHTT) with expanded polyglutamine tract (polyQ) [2,3]. mHTT cytotoxicity is the major cause of HD, while the underlying molecular mechanisms remain unclear and likely involve multiple pathways [2]. Recently, gene therapy approaches targeting *HTT* mRNA have obtained tremendous success in developing potential treatment for HD: in several mammalian models, delivery of short hairpin RNAs (shRNAs) or small interference RNAs (siRNAs) or antisense oligonucleotides (ASOs) targeting *HTT* mRNA lowered *HTT* protein levels and attenuated neuropathology and disease-related phenotypes [4–7]; More importantly, an ASO targeting *HTT* mRNA, *HTT*-Rx developed by IONIS, has been investigated in clinical studies and obtained preliminary success in Phase I/IIa clinical trial [8]. Meanwhile, how *HTT* mRNA is regulated endogenously has been less well understood. This mechanism may worth studying because it may provide novel insights into *HTT* biology and potential therapeutic targets for HD.

The stability of *HTT* mRNA could be influenced by non-coding RNAs including an anti-sense lncRNA expressed by the reverse strand of the *HTT* gene [9]. On the other hand, RNA-binding proteins (RBPs) have been shown to modulate

the stability of many mRNAs by interacting with them, playing key roles in many neurodegenerative disorders such as ALS/FTD [10]. Thus, whether and which RBPs regulate *HTT* mRNA is of interest in the HD and the RNA stability research field and yet remains unknown.

We have previously demonstrated MAPK11 as a novel kinase modulator of *HTT* mRNA stability [11], giving us an entry point to identify potential RBPs regulating *HTT* mRNAs. In this study, we identified HuR as the RBP that interacts with *HTT* mRNA and stabilizes it. We further elucidated relevant molecular mechanisms and the binding site, providing novel insights into *HTT* mRNA regulation and new pathobiology function of HuR.

Results

The RBP HuR is a potential modifier of HTT mRNA levels in HD cells in an mHTT-dependent manner

Our previous studies have shown that MAPK11 modulates the stability of *HTT* mRNA. To identify the potential downstream RBP(s) that interact with *HTT* mRNA, we investigated candidate RBPs that may interact with *HTT* mRNA based on the CLIP-seq data analysed by StarBase (<http://starbase.sysu.edu.cn/>) [12] (Fig. 1A). We then checked the brain expression of this panel of candidate RBPs based BioGPS (<http://biogps.org>) [13] and

CONTACT Boxun Lu  luboxun@fudan.edu.cn  Neurology Department at Huashan Hospital, State Key Laboratory of Medical Neurobiology and MOE Frontiers Center for Brain Science, Institutes of Biomedical Sciences, School of Life Sciences, Fudan University, Shanghai 200438, China; Xiaoli Sun  sunxiaoli@fudan.edu.cn  Shanghai Xuhui District Central Hospital, Zhongshan Xuhui Hospital, Fudan University, Shanghai 200031, China; Lixiang Ma  lxma@fudan.edu.cn  Department of Anatomy, Histology and Embryology, Shanghai Basic Medical College, Fudan University, Shanghai 200032, China

 The supplementary data for this article can be accessed [here](#).

© 2020 The Author(s). Published by Informa UK Limited, trading as Taylor & Francis Group.
This is an Open Access article distributed under the terms of the Creative Commons Attribution-NonCommercial-NoDerivatives License (<http://creativecommons.org/licenses/by-nc-nd/4.0/>), which permits non-commercial re-use, distribution, and reproduction in any medium, provided the original work is properly cited, and is not altered, transformed, or built upon in any way.

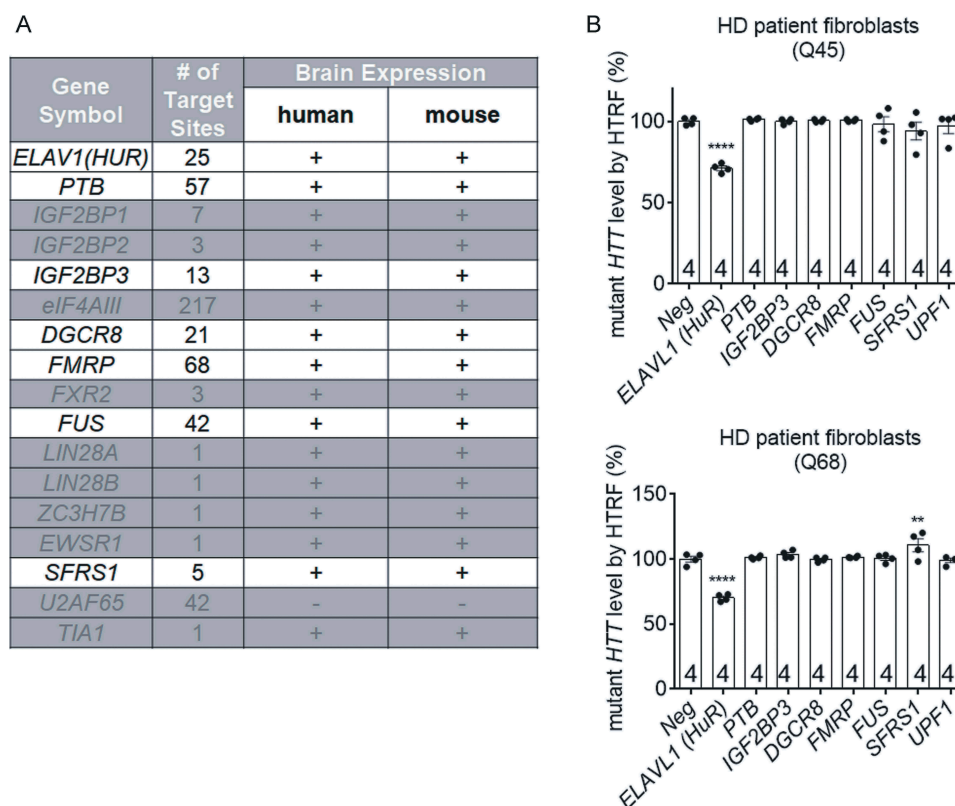


Figure 1. Miniscreen of potential *mHTT* mRNA-interacting RBPs that modulate *HTT* levels.

(A) The list of potential *HTT* mRNA interacting RBPs based on the CLIP-seq data analysed in StarBase (ref. [12]). These candidates were then checked for brain tissue expression at BioGPS (ref. [13]). The ‘# of target sites’ indicate the number of potential RBP-bound sequences detected in the *HTT* mRNA. The RBPs that are expressed in the brain with the ‘# of target sites’ >5 were prioritized for further testing (white rows). *eIF4AIII* was deprioritized since it is a translation initiation factor and may have non-specific effects. (B) *mHTT* levels in the HD patient fibroblasts were tested by HTRF using the 2B7/MW1 antibody pair. Two different lines (Q45 and Q68) were transfected with the pooled siRNA targeting the indicated RBPs. Bars indicate mean and SEM (4 biological replicates). The statistical analysis was performed by one-way ANOVA with the Dunnett’s post hoc tests. **** $P < 0.0001$, ** $P < 0.001$.

selected those brain-expressing RBPs with more than 5 potential *HTT* mRNA targeting sites for further testing (Fig. 1A). We then investigated their potential influences on *mHTT* levels in immortalized HD patient fibroblasts (Q45 and Q68) by the well-established HTRF (homogeneous time-resolved fluorescence) assay using the 2B7/MW1 antibody pair. Transfection of pooled siRNA targeting *ELAVL1* (referred to as ‘*HuR*’ in the subsequent text to keep consistency with the literature), but not the other RBP expressing genes significantly lowered *mHTT* levels in both Q45 and Q68 patient fibroblasts (Fig. 1B), revealing *HuR* as a candidate RBP that regulates *HTT* mRNA.

To confirm *HuR* as an *HTT* mRNA regulator, we tested the effect of *HuR* knockdown in HD cells including the HD knockin mouse striatal cells *STHdh*^{Q7/Q111} [14] and immortalized human HD patient fibroblasts (Q47), which express endogenous full-length mouse homolog of *HTT* (*msHTT*) and human *HTT* (*hsHTT*) mRNA, respectively. *HuR* knockdown by siRNAs significantly reduced *HTT* mRNA levels in both cell lines (Fig. 2A, B, note that the same set of siRNAs were able to knockdown both human and mouse *HuR* because of their sequence similarities, and thus we used the *HuR* symbol for both mouse and human cells; knock-down efficiency was also validated by Western-blot in Fig. S1). Consistent with this, *HuR* knockdown in other HD patient fibroblast lines (Q45 & Q68) reduced *HTT* mRNA levels as well (Fig. S2). Consistently, *HuR* knockdown lowered *HTT* protein levels as well (Fig. 2C). On the other hand, over-expression of *HuR*

by cDNA transfection in the *STHdh*^{Q7/Q111} significantly increased *HTT* mRNA levels (Fig. 2D), confirming *HuR* as a positive regulator of *HTT* mRNA levels.

Interestingly, the *HuR*-mediated *HTT* mRNA regulation seemed to be missing in the wild-type cells (Fig. 2A, B). This could be explained by two possibilities. First, *HuR* only regulates mutant *HTT* mRNA with expanded CAG repeats. Second, *HuR* regulates both mutant and wild-type *HTT* mRNA, but the regulation is dependent on the presence of the mutant *HTT* mRNA and/or protein.

To distinguish between these two possibilities, we exogenously expressed mutant *hsHTT* mRNA and proteins in the wild-type mouse cells (*STHdh*^{Q7/Q7}), in which the endogenous wild-type *msHTT* mRNA level was insensitive to *HuR* knockdown. Expression of full-length mutant *hsHTT* (*hsHTT*-Q73) or the mutant *hsHTT*-exon1 fragment (*hsHTT*-exon1-Q72) enabled the *HuR* to regulate the endogenous wild-type *msHTT* mRNA, whereas expressing wild-type *hsHTT* had no effects (Fig. 2E), validating the second possibility. Thus, *HuR* may regulate both mutant and wild-type *HTT* mRNA, but in a mutant *HTT* dependent manner.

HuR positively regulates *HTT* mRNA stability

As a member of the ELAVL family RBPs, *HuR* may stabilize target mRNAs by its direct interaction with them [15]. Thus,

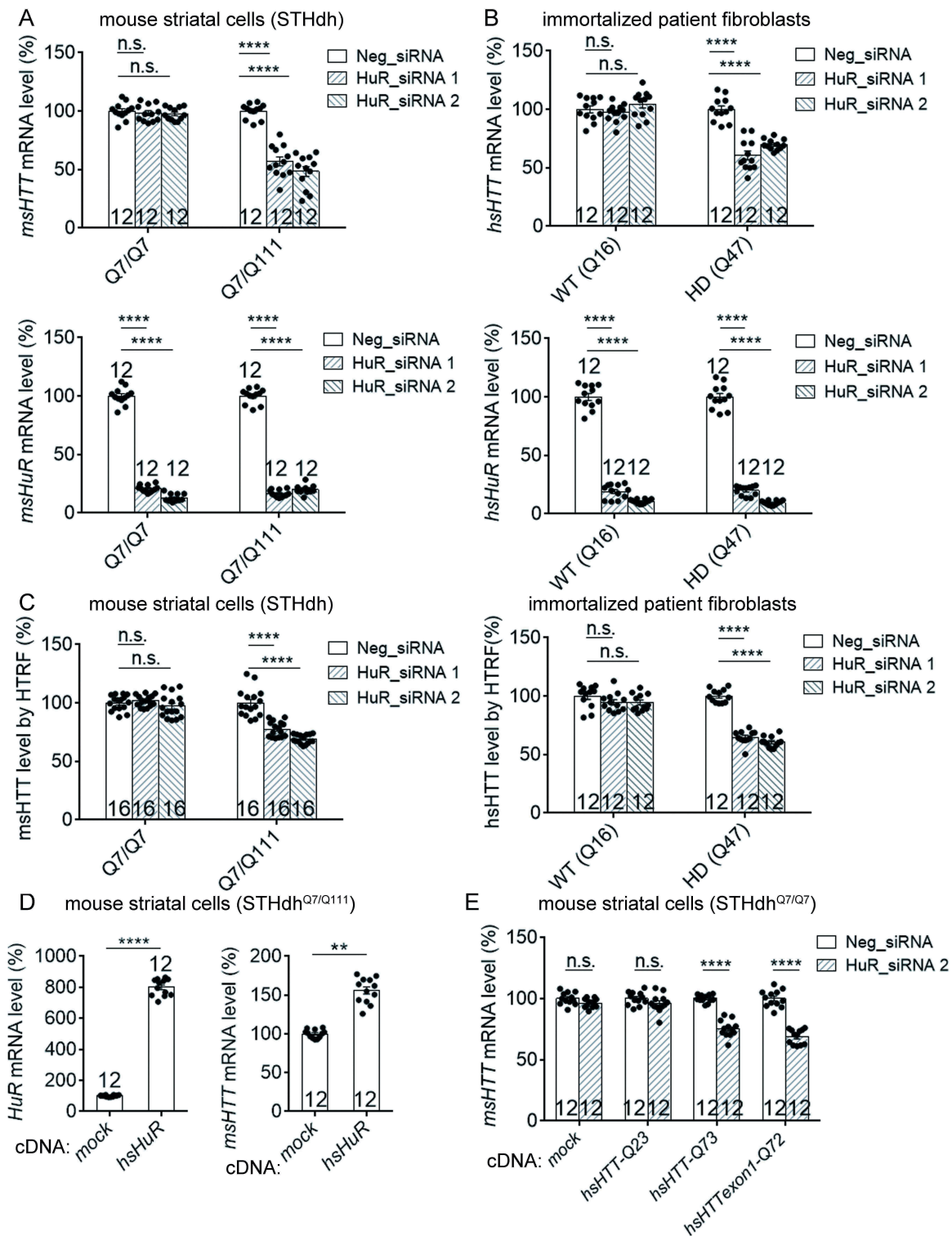


Figure 2. HuR modulates *HTT* mRNA levels in a mHTT dependent manner.

(A) RT-qPCR measurements of *HuR* and *HTT* mRNA level in wild-type (STHdh^{Q7/Q7}) or HD (STHdh^{Q7/Q111}) mouse striatal cells transfected with the siRNAs targeting *HuR* (HuR_siRNA 1 and HuR_siRNA 2) or with the non-targeting control siRNA (Neg_siRNA) for 48 hours (12 technical replicates from 3 biological replicates). All signals were normalized to the averaged signal of Neg_siRNA transfected controls. (B) Similar to (A), but in immortalized human wild-type (Q16) or HD (Q47) fibroblasts (12 technical replicates from 3 biological replicates). (C) HTRF measurements of HTT protein levels in the HuR siRNA or the non-targeting control siRNA (Neg_siRNA) transfected wild-type or HD cells (12 technical replicates from 3 biological replicates for STHdh cells, and 16 technical replicates from 4 biological replicates for immortalized human fibroblasts). The siRNAs were transfected for 72 hours. All signals were normalized to the Neg_siRNA transfected controls. Note that the HTRF antibody pair 2B7/2166 was used here to detect the total HTT (including mHTT and wild-type HTT proteins) levels, different from the mHTT-specific antibody pair used for Fig. 1B. (D) RT-qPCR measurements of *HuR* and mouse *HTT* (*msHTT*) mRNA levels in the HD mouse striatal cells (STHdh^{Q7/Q111}) transfected with cDNA plasmids expressing human *HuR*. All signals were normalized to the averaged signal of the empty vector transfected control group (mock) (12 technical replicates from 3 biological replicates). Note that the *HuR* mRNA measurement in the mock group utilized the mouse *HuR* qPCR primers, whereas the one in the *HuR* transfected group utilized human *HuR* qPCR primers. Since these two sets of primers had similar efficiency (Fig. S5) and the same threshold was used for analysis, the comparison between these two groups is valid. (E) RT-qPCR measurements of *HuR* and mouse *HTT* (*msHTT*) mRNA level in the wild-type mouse striatal cells (STHdh^{Q7/Q7}). The cells were transfected with the siRNAs targeting *HuR* or the non-targeting control siRNA (Neg_siRNA), and then after 24 hours with cDNA plasmids expressing human wild-type full-length HTT (*hsHTT-Q23*), mutant HTT exon1 (*hsHTTExon1-Q72*) or full-length (*hsHTT-Q73*) (12 technical replicates from 3 biological replicates). The mRNA levels were then measured 48 hours after cDNA transfection. All the signals were normalized to the averaged signals of the Neg_siRNA transfected control groups. For all plotted data, error bars represent mean and SEM. The statistical analysis was performed by one-way ANOVA and post-hoc Dunnett's tests for A-C, and two-tailed unpaired t tests for D-E. **P < 0.01; ****P < 0.0001; n.s., P > 0.05.

the most likely mechanism of HuR-mediated regulation of *HTT* mRNA levels is *via* RNA-stabilization. We thus examined *HTT* mRNA degradation in the HD cells by measuring the levels of mRNAs after treatment of actinomycin D, which stops new RNA synthesis by inhibiting RNA polymerase activity so that the degradation of pre-existing mRNAs could be measured by qPCR directly. In HD cells, including STHdh^{Q7/Q111} and immortalized human patient fibroblasts (Q47), transfection of *HuR* siRNAs significantly increased the degradation of *HuR* mRNA *via* RNA interference (Fig. 3A, B, left panels). Importantly, both *msHTT* and *hsHTT* mRNAs were also degraded significantly faster in *HuR* knockdown cells than in the control cells, suggesting that HuR is required for *HTT* mRNA stabilization in these cells (Fig. 3A, B, right panels).

To further confirm this conclusion, we attempted to knock out the *HuR* gene in STHdh^{Q7/Q111} cells by the CRISPR/cas9 system, but only managed to obtain pooled colonies of heterozygous *HuR* knockout cells (*HuR*[±], Fig. 3C), possibly because a complete loss of *HuR* is cytotoxic. The *HTT* mRNA degradation in the *HuR*[±] STHdh^{Q7/Q111} cells was also significantly faster than in the *HuR*^{+/+} STHdh^{Q7/Q111} cells (Fig. 3C), consistent with the knockdown experiments. Taken together, HuR positively regulates *HTT* mRNA levels *via* increasing its stability.

The HuR protein interacts with HTT mRNA in its exon 11 in the coding region

As an RBP, HuR may directly interact with *HTT* mRNA to stabilize it. In fact, previous PAR-CLIP-Seq data analysed in Starbase [12] suggested 25 potential HuR-binding sites on human *HTT* mRNA (Fig. 4A). To confirm the binding between HuR and the *HTT* mRNA, we performed RNA-immunoprecipitation (RNA-IP) experiments in STHdh^{Q7/Q111} and immortalized Q47 fibroblasts. The HuR protein was pulled down by anti-HuR conjugated magnetic beads, and the amount of *HTT* mRNA that was pulled down with the HuR protein was remarkably higher than the control (pulled down by IgG-conjugated beads) (Fig. 4B), suggesting that the HuR protein interacts with *HTT* mRNA in these HD cells.

We further explored the HuR-binding site(s) in the *HTT* mRNA. Based on the analysis of StarBase (Fig. 4A), some of the potential binding sites are in the coding region, whereas some are in the 3'-UTR. Thus, we exogenously expressed *hsHTT* cDNA with only the coding sequence but not the 3'UTR sequence to test if at least some of the binding site(s) are within the coding region. We transfected the wild-type mouse STHdh^{Q7/Q7} cells with the plasmids that exogenously express human mutant HTT with full-length coding sequences (CDS) (*hsHTT-Q73*) or with exon 1 only (*hsHTTExon1-Q72*), and performed RNA-IP experiments for the exogenously expressed *hsHTT* mRNAs (not the endogenous *msHTT* mRNA) to test whether the HuR protein can bind with them. The empty vector transfected control sample (mock) did not give any *hsHTT* signals (Fig. 4C), confirming that the RNA-IP experiments and qPCR measurements only detect the binding to exogenously expressed *hsHTT* mRNAs. The HuR antibody- and

IgG-conjugated beads pulled down similar levels of the *hsHTTExon1-Q72* mRNA (Fig. 4C), suggesting that the binding site(s) are probably not within the exon 1 region. In comparison, the HuR was able to bind with the mutant full-length *hsHTT* CDS (Fig. 4C, *hsHTT-Q73*), suggesting that at least some of the binding site(s) are within the coding region. Interestingly, no binding with the wild-type full-length *hsHTT* CDS (Fig. 4C, *hsHTT-Q23*) was detected, suggesting that the binding is dependent on the presence of mHTT, consistent with previous functional experiments (Fig. 2E). To further test if this binding is functionally relevant, we knocked down *HuR* mRNA in these cells and tested if these exogenously expressed *hsHTT* mRNA levels were influenced. Consistent with the RNA-IP data, only the levels of full-length mutant *HTT* CDS mRNA (*hsHTT-Q73*) were significantly reduced by *HuR* knockdown, but not the ones of its exon 1 fragment mRNA (*hsHTTExon1-Q72*) or the wild-type full-length *HTT* CDS (*hsHTT-Q23*) (Fig. 4D). Collectively, our data suggest that HuR functionally interacts with the *HTT* mRNA in its protein coding region, but not in its exon 1.

To map the precise binding site(s), we reviewed all the potential binding sites based on StarBase (Fig. 4A) and blasted these sequences with the *msHTT* mRNA to see whether these sites are conserved between human and mouse, because HuR was able to interact with both *hsHTT* and *msHTT* to regulate their stability (Figs. 2 & 3). We found that only one candidate site, #105708, has conserved sequences between human and mouse (Fig. 4A, highlighted). Thus, #105708 is likely a HuR-binding site that mediates HuR's regulation of *HTT* mRNA stability. Since #105708 locates in exon 11 of the *HTT* mRNA, we tested if exon 11 is required for the interaction between HuR and the *HTT* mRNA. Thus, we constructed two plasmids expressing the first 10 (exon 1–10) or 11 exons (exon 1–11) of the mutant human *HTT* mRNA (*hsHTT-Q73*), respectively. The only difference between these two plasmids is the presence of exon 11. We then transfected the wild-type mouse STHdh^{Q7/Q7} cells with these plasmids to test whether HuR could bind to the mRNAs expressed by these two plasmids. RNA-IP experiment results showed that the HuR protein interacted with exon 1–11, but not exon 1–10 (Fig. 5A), suggesting that the binding site is within the exon 11 region and likely to be #105708.

To confirm this, we cloned several candidate sequences (including #105708) into the *EGFP* construct, so that the 3' UTR of *EGFP* mRNA contains these sequences. We then transfected the HD mouse STHdh^{Q7/Q111} cells with these plasmids and tested whether HuR may interact with the *EGFP* mRNAs expressed from these plasmids. RNA-IP experiments showed that the *EGFP* mRNAs with #105708 sequences (*hs#105708* and *ms#105708* for human and mouse sequences, respectively) but not the #105717 sequence exhibited interaction with HuR (Fig. 5B). The experiment also suggests that #105708 is sufficient for HuR binding in the HD cells.

To further validate #105708 as the binding site, we performed RNA electrophoretic mobility shift assays (R-EMSA) experiments to test the direct interaction between HuR and #105708. We mixed Cy3-labelled RNA oligos of either the human #105708 (*hs#105708*) or the mouse #105708 (*ms#105708*) sequences with the HuR-MBP.His protein (with the human HuR amino acid sequence) purified from HEK293T cells (Fig. S3) at indicated

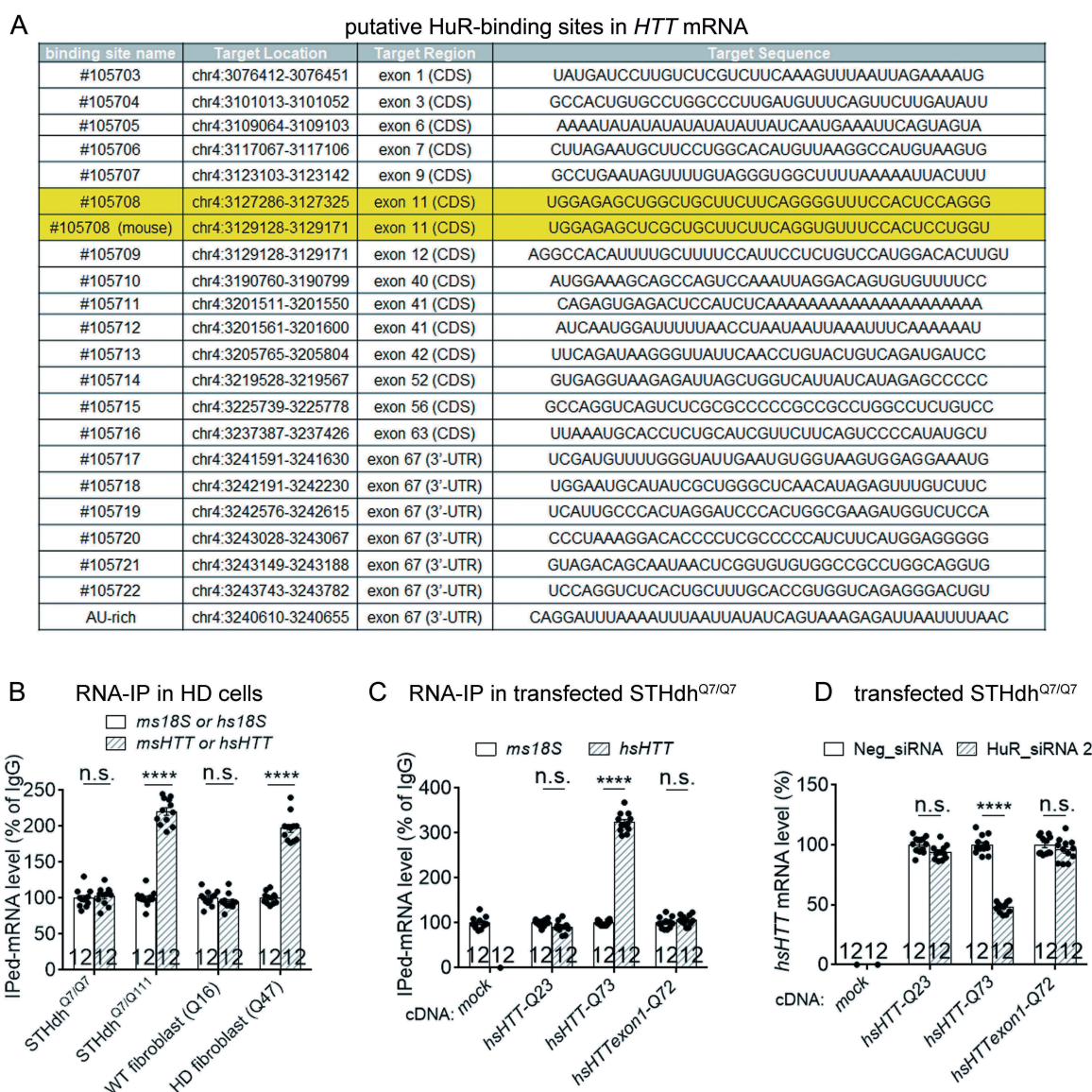


Figure 4. HuR interacts with *HTT* mRNA in the HD cells, likely in the protein-coding region of *HTT*.

(A) A list of potential HuR's binding sites in human *HTT* (*hsHTT*) mRNA based on StarBase (ref. [12]). The highlighted lines indicate a candidate site (#105708) that has conserved sequences in human and mouse. 'AU-rich' indicates a site that is not listed in StarBase, but is still a possible interaction site predicted by HuR preferred binding sequences (ARE). (B) RT-qPCR quantifications of HuR-bound *HTT* mRNA levels in HD mouse striatal cells (STHdh^{Q7/Q111}) or immortalized HD patient fibroblasts (Q47) as well as the wild-type controls (STHdh^{Q7/Q7} and Q16) by RNA-IP (12 technical replicates from 3 biological replicates). IgG was used as a negative control for the IP, and the 18S level was quantified as a baseline control to normalize the signals. (C) RT-qPCR quantifications of HuR-bound exogenously expressed human *HTT* (*hsHTT*) mRNA levels in WT mouse striatal cells (STHdh^{Q7/Q7}) transfected with cDNA plasmids expressing full-length wild-type human *HTT* (*hsHTT-Q23*), full-length mutant *HTT* (*hsHTT-Q73*) or exon1 of mutant *HTT* (*hsHTTExon1-Q72*) by RNA-IP (12 technical replicates from 3 biological replicates). IgG was used as a negative control for the IP, and the 18S level was quantified as a baseline control to normalize the signals. (D) RT-qPCR quantifications of the exogenously expressed human *HTT* mRNA level in wild-type mouse striatal cells (STHdh^{Q7/Q7}) transfected with the *HuR* siRNA or the non-targeting control siRNA (Neg_siRNA). The cDNA plasmids expressing exon1 (*hsHTTExon1-Q72*) or full-length (*hsHTT-Q73*) of human mutant *HTT* mRNA were transfected 24 hours after siRNA transfection, and their levels were measured after another 48 hours (12 technical replicates from 3 biological replicates). For all plotted data, error bars represent mean and SEM. The statistical analysis was performed by two tailed unpaired t tests, *****P* < 0.0001; n.s.: *P* > 0.05.

ratios and ran the samples on native-PAGE gels (Fig. 5C). We observed apparent molecular weight-shift of these RNA oligos due to mobility block caused by HuR binding (Fig. 5C), suggesting that HuR interacts with both mouse and human #105708 sequences directly, consistent with the RNA-IP results (Fig. 5B). As controls, we performed R-EMSA for an RNA oligo with known HuR-interacting sequence (Fig. 5C, Cxcl 2) [16], and observed expected apparent molecular weight shift as well. In addition, we tested two other candidate binding sites using R-EMSA. #105717 is a candidate binding site in the 3' UTR region

(Fig. 4A). The 'AU-rich' oligo contains the only AU-rich element (ARE) in the *HTT* mRNA. Since AREs are the HuR preferred binding sites [15], we anticipated that the 'AU-rich' oligo might interact with HuR as well. Surprisingly, we observed no apparent molecular weight shift of RNA oligos with either of these two sequences (Fig. 5C), suggesting that #105708 is a relatively specific site in the *HTT* mRNA for HuR binding.

To investigate whether the HuR-#105708 interaction is functional in regulating mRNA levels in the cells, we cloned candidate binding site sequences into a firefly-renilla dual-luciferase

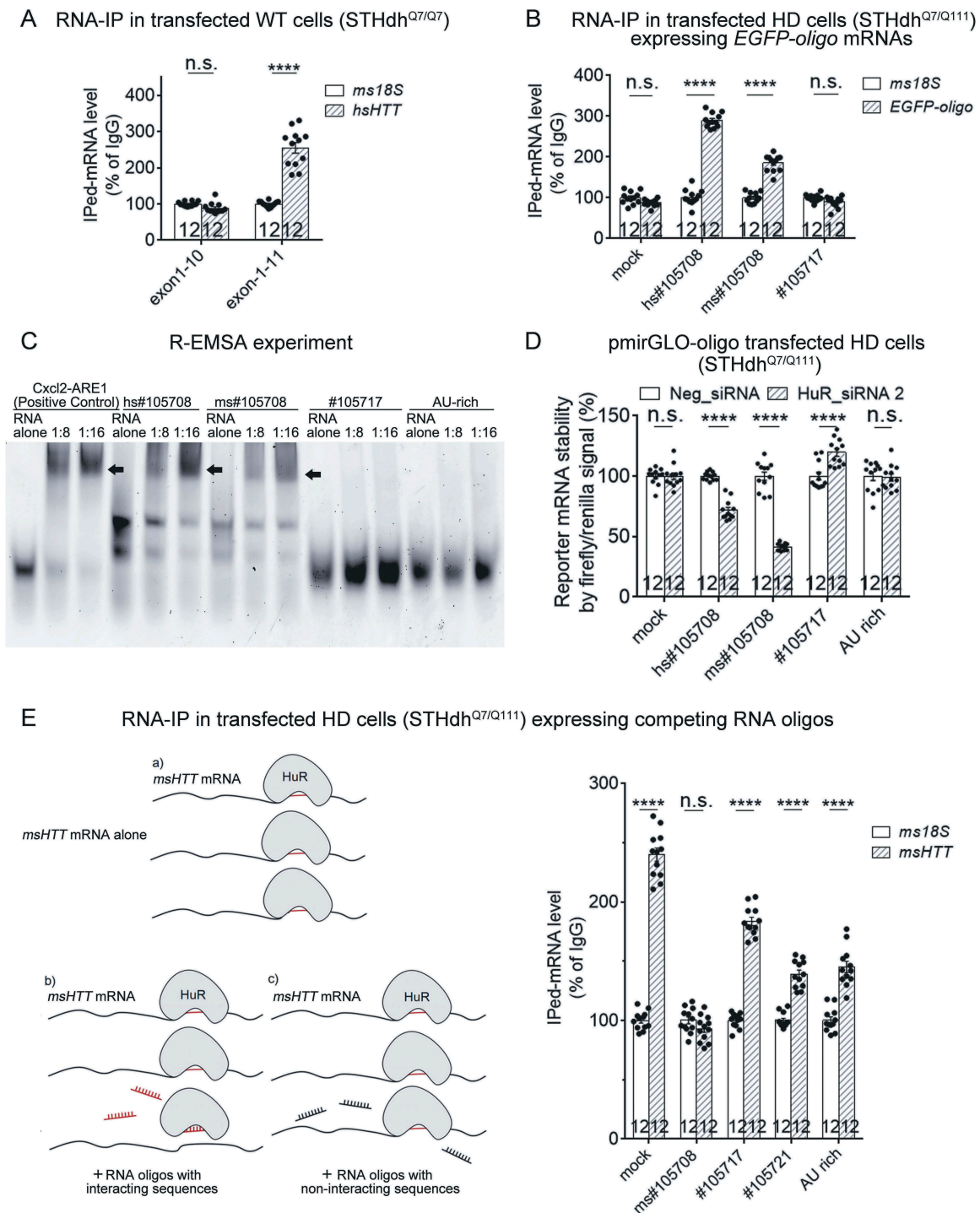


Figure 5. HuR interacts with #105708 site in exon 11 of the *HTT* mRNA.

(A) RT-qPCR quantifications of HuR-bound exogenously expressed *HTT* mRNA 5' fragment (exon 1–10 or exon 1–11) levels in the wild-type mouse striatal cells (STHdh^{Q7/Q7}) by RNA-IP (12 technical replicates from 3 biological replicates). IgG was used as a negative control for the IP, and the 18S level was quantified as a baseline control to normalize the signals. HuR interacted with exon 1–11 but not exon 1–10, suggesting that exon 11 contains the HuR-binding site. (B) Similar to (A), but in HD cells (STHdh^{Q7/Q111}) transfected with cDNA plasmids expressing EGFP mRNAs containing different candidate binding sites in its 3' UTR region (12 technical replicates from 3 biological replicates). The EGFP mRNA with #105708 site sequences (mouse or human) showed interaction with HuR, suggesting that #105708 (located in exon 11 of *HTT* mRNA) is a potential HuR-binding site. (C) A representative R-EMSA gel image of different Cy3-labelled RNA oligos of potential binding site sequences after co-incubation with purified HuR-MBP.His proteins (see Fig. S3). The first lanes in each group were loaded by the indicated RNA oligos alone. In the 2nd and 3rd lanes in each group, the indicated RNA oligos were incubated and loaded with purified HuR-MBP.His protein at different concentration ratios as indicated. Five repeats were performed, showing consistent results. HuR-binding with the RNA oligo leads to an apparent molecular weight shift to the top (dark arrows), due to mobility block caused by protein-binding. (D) Quantification of the ratio between firefly luciferase and renilla luciferase signals in HD mouse striatal cells (STHdh^{Q7/Q111}) transfected with the pmirGLO reporter plasmids (12 technical replicates from 3 biological replicates). The firefly/renilla signal ratio is an indicator of the level of firefly luciferase mRNA, of which the 3' UTR region contained different sequences of potential HuR-binding sites. The HuR knockdown by siRNA caused lowering of the firefly/renilla signal ratio only for #105708-containing plasmids, suggesting that #105708 is likely a functional binding site. (E) RT-qPCR quantifications of HuR-bound endogenous mouse *HTT* (*msHTT*) mRNA levels in HD mouse striatal cells (STHdh^{Q7/Q111}) transfected with pmirGLO plasmids expressing firefly luciferase mRNAs containing different potential binding sites (12 technical replicates from 3 biological replicates). The mRNAs with functional binding sites may compete with endogenous *msHTT* mRNA for HuR binding (illustrated in the schematic picture in the left panel). Thus, the RNA-IP signals of the corresponding samples could be reduced (right panel). IgG was used as a negative control for the IP, and the 18S level was quantified as a baseline control to normalize the signals. For all plotted data, error bars represent mean and SEM. The statistical analysis was performed by two-tailed unpaired t tests, ****P < 0.0001; n.s.: P > 0.05.

plasmid (pmirGLO). The 3'UTR of its expressed *firefly luciferase* mRNA contains the sequence of every single candidate binding site, whereas the renilla luciferase was expressed by an independent promoter in the same plasmid as an internal control. Thus, the firefly luciferase signal divided by the renilla luciferase signal (firefly/renilla signal) reflects the relative level of *firefly luciferase* mRNA containing each individual candidate binding site, and this ratio serves as readout for mRNA stability. We thus transfected these plasmids into the mouse HD cells (STHdh^{Q7/Q111}) and tested the effect of HuR knockdown. Among all the candidate sequences tested in this reporter assay, only the #105708 (hs#105708 and ms#105708) sequences caused significantly decreased firefly/renilla signal after HuR knockdown (Fig. 5D), suggesting that the HuR-#105708 interaction is functional in regulating mRNA levels in the HD cells.

Finally, we tested if the #105708-containing mRNA may compete with endogenous *HTT* mRNA for HuR's binding (Fig. 5E, see the schematic picture in the left panel). If so, #105708 RNA oligos may serve as potential reagents to decrease mutant *HTT* RNA stability for HD research and possible therapeutic intervention. Exogenous expression of #105708 containing *firefly luciferase* mRNA largely blocked the interaction between endogenous HuR proteins and the *HTT* mRNA, based on the RNA-IP experimental results (Fig. 5E, right panel), validating the competition effects of #105708. As controls, this phenomenon was not observed for *firefly luciferase* mRNAs containing other candidate HuR binding sequences (Fig. 5E, right panel). Collectively, HuR interacts with the *HTT* mRNA directly at the #105708 site in its exon 11 region *in vitro* and in the HD cells, and this interaction is functional in regulating target mRNA levels.

HuR interacts with *HTT* mRNA in a mHTT-dependent manner via MAPK11

Interestingly, the HuR-*HTT* mRNA interaction was not detected in wild-type cells, where mHTT was not present (Fig. 6A, mock; Fig. 4B, STHdh^{Q7/Q7} & Q16; Fig. 4C, *hsHTT-Q23*). This is consistent with the observation that HuR regulates both mutant and wild-type *HTT* mRNA in a mutant *HTT* dependent manner (Fig. 2A-E). We thus tested if the HuR-*HTT* mRNA interaction is also dependent on the presence of mHTT. We transfected wild-type mouse cells (STHdh^{Q7/Q7}) with plasmids expressing mHTT (*hsHTT-Q73*) or its exon 1 fragment (*hsHTTExon1-Q72*) or the empty control plasmid (mock), and then performed the RNA-IP experiments similar to previously presented in Fig. 4C, but testing HuR's interaction with the endogenous mouse *HTT* mRNA (*msHTT*) at this time (Fig. 6A). Expression of mHTT or its exon 1 fragment restored the originally missing interaction between HuR and the wild-type *HTT* mRNA (Fig. 6A, *hsHTT-Q73* and *hsHTTExon1-Q72* compared with mock), confirming the mHTT-dependence of HuR's binding to the *HTT* mRNA.

We further confirmed this by testing the functional consequence of the HuR-#105708 interaction using the dual-reporter assay. The firefly/renilla signal was not influenced by HuR knockdown in wild-type cells (STHdh^{Q7/Q7}), even for #105708 containing pmirGLO plasmids (Fig. 6B), suggesting

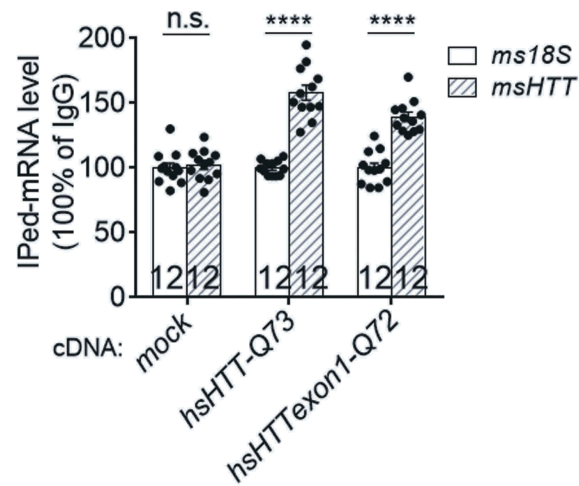
that the HuR-#105708 interaction is absent in the wild-type cells, different from the one observed in HD cells (Fig. 5D). However, when these cells were transfected with the mHTT exon 1 fragment (*hsHTTExon1-Q72*), the firefly/renilla signal in the #105708-containing group became sensitive to the HuR knockdown (Fig. 6C), confirming that mHTT expression is sufficient to drive the HuR-#105708 interaction. Taken together, the interaction between HuR protein and *HTT* mRNA is dependent on the presence of mHTT.

HuR locates in both the nuclei and cytoplasm, and shuttles between the two cellular compartments [17]. Since HuR mainly locates in the nuclei but stabilize mRNA in the cytoplasm [18], we hypothesize that it distributes more in the cytoplasm in the HD cells or the presence of mHTT, so that it interacts and regulates the *HTT* mRNA in an mHTT-dependent manner. Consistent with this hypothesis, the cytoplasmic localization of HuR is significantly higher in the mouse HD cells (STHdh^{Q7/Q111}) compared to the one in wild-type cells (STHdh^{Q7/Q7}), based on the Western-blots of cytoplasmic versus nuclear fractions of these cells (Fig. 7A). A similar phenomenon was observed *in vivo* in the striatal tissue from 6.5-month-old HD versus wild-type mice (Fig. 7B). To confirm the enhanced cytoplasmic localization of HuR, we immunostained the HuR protein in wild-type (STHdh^{Q7/Q111}) versus HD (STHdh^{Q7/Q111}) cells to investigate its cellular distribution by high-content confocal imaging technology. Imaging analysis of thousands of cells showed that the cytoplasmic to nuclear ratio of HuR protein is significantly higher in the HD than the wild-type cells (Fig. 7C), consistent with the biochemical fractionation experiments (Fig. 7A, B). Finally, to functional characterize the increased cytoplasmic localization of HuR in the HD cells, we performed RNA-IP in both wild-type and HD cells to test the HuR-bound *HTT* mRNA levels in nuclear versus cytoplasmic fractions. The cytoplasmic HuR bound *HTT* mRNA level was significantly higher in the HD cells than the wild-type ones (Fig. 7D), consistent with the increased cytoplasmic localization of HuR in HD cells.

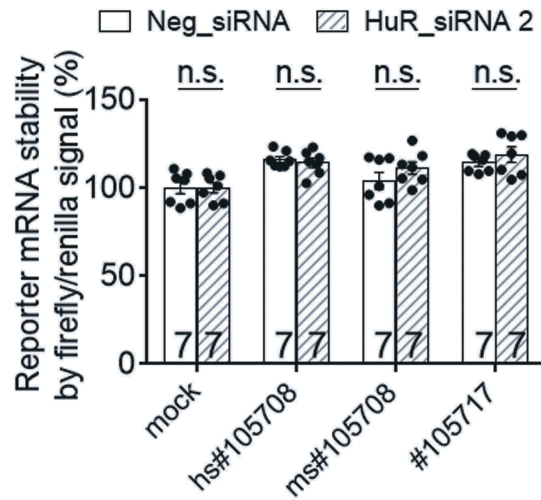
We then investigated the potential mechanism of the higher cytoplasmic localization of HuR in the HD cells. Our previous work identified MAPK11 as a positive modulator of *HTT* mRNA stability [19] and it is also activated by mHTT [20]. In addition, MAPK11 belongs to the p38 MAPK family, which are able to enhance HuR levels and activate cytoplasmic translocation of HuR [21], although the exact member(s) of this family that makes a major contribution to this function is yet to be identified. We thus hypothesized that mHTT may activate MAPK11 to enhance the cytoplasmic localization of HuR, which may then interact with and stabilize the *HTT* mRNA.

To test this hypothesis, we performed epistatic experiments to test if HuR is downstream of MAPK11 in regulating *HTT* mRNA levels. Consistent with our previous observation [19], knockdown of mouse MAPK11 (msMAPK11) significantly reduced *HTT* mRNA levels in the HD cells (STHdh^{Q7/Q111}) (Fig. 8A). Meanwhile, knockdown of HuR largely abolished this effect, suggesting that HuR is downstream of MAPK11 in regulating *HTT* mRNA levels (Fig. 8A). Consistently, lowering HuR by knockdown or heterozygous knockout significantly

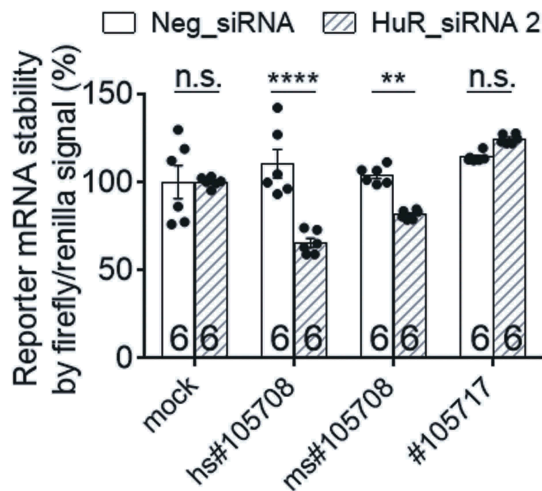
A RNA-IP in WT cells (STHdh^{Q7/Q7})



B pmirGLO transfected WT cells (STHdh^{Q7/Q7})



C pmirGLO + HTTExon1-Q72 transfected WT cells (STHdh^{Q7/Q7})



ameliorated MAPK11's effects on the *HTT* mRNA stability in both mouse (STHdh^{Q7/Q111}) and human HD cells (Q47) (Fig. 8B–D), confirming that HuR is likely downstream of MAPK11 in stabilizing the *HTT* mRNA.

We thus further investigated whether MAPK11 influences HuR's cytoplasmic localization. MAPK11 knockdown significantly reduced cytoplasmic localization of HuR based on the Western-blots of cytoplasmic versus nuclear fractions of mouse HD cells STHdh^{Q7/Q111} (Fig. 9A), illustrating that MAPK11 regulates the nuclei-cytoplasm distribution of HuR. Consistently, knockout of the mouse *MAPK11* (*msMAPK11*^{-/-}) significantly reduced the cytoplasmic/nuclear ratio of HuR in the 6.5-month-old HD mouse (Hdh^{Q140/Q140}) striatal tissue as well, confirming that MAPK11 regulates HuR's cytoplasmic localization as well (Fig. 9B). Consistent with this, MAPK11 knockdown reduced HuR cytoplasmic localization (Fig. 9C) as well as the cytoplasmic HuR-bound *HTT* mRNA level (Fig. 9D, in which the IPed *msHTT* mRNA in the cytoplasmic fraction of HD cells was obviously lowered by *Mapk11_si* transfection comparing to *Neg_si* transfected controls) in the HD cells. Taken together, the most likely interpretation of our data is that the presence of mHTT activates MAPK11 [19,20], which then induces cytoplasmic translocation of HuR. HuR then binds to the #105708 sequence in exon 11 of *HTT* mRNA and stabilizes it (Fig. 10). Thus, MAPK11 or HuR knockdown destabilizes the *HTT* mRNA in an mHTT-dependent manner.

Discussion

In this work, we identified HuR as a novel RBP that modulates *HTT* mRNA stability in HD cells. To our knowledge, it is the first reported RBP that interacting with and stabilizing the *HTT* mRNA.

The interaction between HuR and *HTT* mRNA is non-canonical in several ways, which may provide additional insights into HuR biology. It interacts with a non-AU-rich sequence in the coding region, instead of the canonical ARE in the 3'-UTR (Fig. 5). This type of interaction could be loose, compared to canonical ones, so that it does not interfere with protein translation. Meanwhile, this coding-region and non-AU-rich type of HuR interaction is still functional in stabilizing the target mRNA, consistent with a very recent HuR study [22].

Another interesting feature of HuR's interaction with the *HTT* mRNA is that the interaction is dependent on the presence of mHTT DNA, RNA or protein (Fig. 6). The mHTT protein is likely the major contributor to activate HuR's interaction with the *HTT* mRNA, because we utilized mixed CAGCAA sequences in the mHTT-expressing cDNA plasmids (Figs. 4C, D & 6B, C), which lacked the expanded CAG repeat sequences required to

induce DNA replication errors or RNA foci formation or RNA phase separation [23,24]. Thus, it is more likely that the mHTT protein enabled HuR's capability in regulating the *HTT* mRNA, possibly *via* activating MAPK11 (Figs. 8 & 9). Taken together, the mHTT-MAPK11-HuR-*HTT* mRNA pathway may form a positive feedback loop (Fig. 10), which may accelerate mHTT protein accumulation and contribute to HD progression over time.

The therapeutic potential of the pathway remains to be tested. While targeting the *HTT* mRNA by siRNA, shRNA or ASOs provides extremely promising strategies for HD treatment [25], these approaches require delivery of large biomolecules or viral particles such as AAV, which is challenging and expensive. In addition, these exogenously delivered large biomolecules or viruses might activate certain biological responses such as the interferon response that might be risky in certain circumstances. A very recent study has also shown that the CAG repeat number rather than polyQ length might determine the age of onset in HD [26], implying that the CAG repeat containing *HTT* mRNA may play a more important role than previously thought. Targeting the *HTT* mRNA by MAPK11/HuR provides a possible alternative approach for HD drug development. Both MAPK11 and HuR have reported inhibitors [27,28], which could be used to test the therapeutic potential of this pathway. In fact, our previous reports suggested that the MAPK11 inhibitor SB202190 may reduce mHTT levels to rescue HD-relevant phenotypes in the HD neurons [19], although the HuR inhibitors are unavailable to us. Meanwhile, further optimization of MAPK11 and/or HuR inhibitors may provide small compound drugs lowering the *HTT* mRNA to treat HD.

Besides the involvement of mHTT in HD, the wild-type HTT protein is also an important protein that is essential during development and plays critical roles in various cellular functions [29]. As an *HTT* mRNA modulator, HuR may participate in key biological functions *via* regulating the wild-type HTT as well. In our study, HuR-mediated modulation of *HTT* mRNA levels is dependent on the presence of mHTT, but it is possible that this regulation is activated under some other pathophysiological or even physiological conditions. In fact, MAPK11 and other p38 MAPKs are activated by various types of cellular stress such as oxidative, genotoxic, and osmotic stress and by proinflammatory cytokines occurring in many human diseases including neurodegenerative disorders other than HD [30]. Thus, HuR might stabilize the wild-type *HTT* mRNA in those disease neurons to protect them, considering the neuroprotective function of wild-type HTT [31]. Another interesting possibility is the HuR may play a role during development by modulating wild-type HTT. The p38 MAPK pathway is known to be activated during embryonic development [32], whereas wild-type HTT is also

Figure 6. HuR interacts with *HTT* mRNA in an mHTT-dependent manner.

(A) RT-qPCR quantifications of the levels of endogenous mouse *HTT* (*msHTT*) mRNA bound with HuR in WT mouse striatal cells (STHdh^{Q7/Q7}) transfected with empty vector (mock) or cDNA plasmids expressing full-length (*hsHTT-Q73*) or exon 1 (*hsHTTExon1-Q72*) by RNA-IP (12 technical replicates from 3 biological replicates). IgG was used as a negative control for the IP, and the 18S level was quantified as a baseline control to normalize the signals. (B) Similar to Fig. 5D, but in wild-type cells (STHdh^{Q7/Q7}) (7 biological replicates). (C) Similar to Fig. 5D, but in wild-type cells (STHdh^{Q7/Q7}) transfected with *hsHTTExon1-Q72* plasmid 24 hours before transfection of the pmirGLO reporter plasmids with the indicated potential binding sites (6 biological replicates). o-tailed unpaired t tests, ****P < 0.0001; n.s.: P > 0.05. For all plotted data, error bars represent mean and SEM. The statistical analysis was performed by two-tailed unpaired t tests. **P < 0.01; ****P < 0.0001; n.s., P > 0.05.

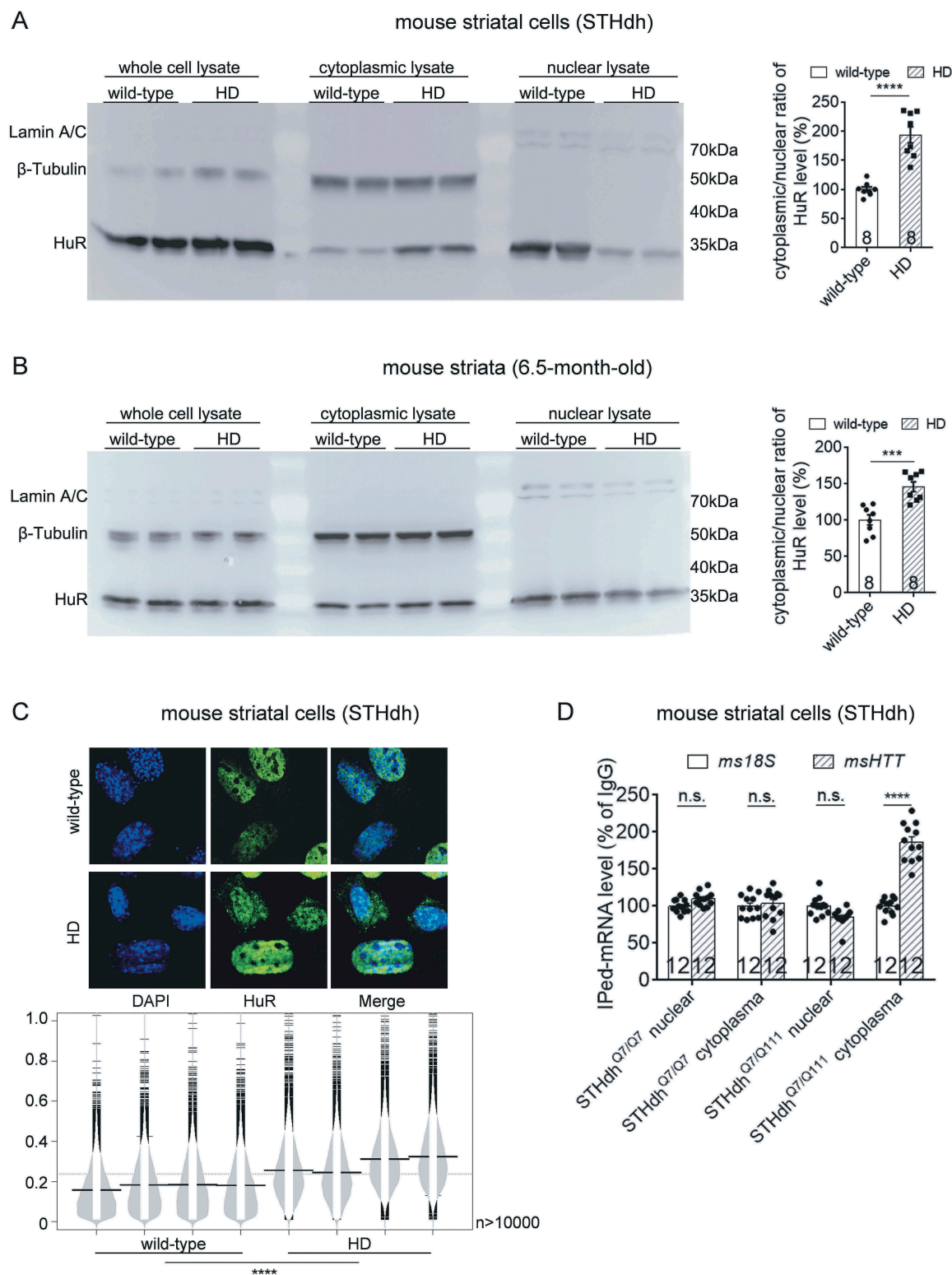


Figure 7. The nuclear/cytoplasmic distribution of HuR protein in wild-type versus HD cells or tissues.

(A) Representative Western-blot (from 4 biological replicates) of HuR protein levels in the nuclear or cytoplasmic fractions of wild-type (STHdh^{Q7/Q7}) or HD (STHdh^{Q7/Q111}) mouse striatal cells. β -Tubulin was blotted as a cytoplasmic loading control, and Lamin A/C as a nuclear loading control. These two control proteins were only detected in their localized fractions, confirming reliable nuclei/cytoplasm separation. The cytoplasmic/nuclear ratios of HuR signals were quantified and plotted (8 technical replicates from 4 biological replicates). (B) Similar to (A), but in the cytoplasmic and nuclear fractions of striatal tissue lysates from 6.5-month-old wild-type (*Hdh*^{Q7/Q7}) or HD (*Hdh*^{Q140/Q140}) mice (8 technical replicates from 4 biological replicates). (C) Representative images and quantifications of immunofluorescent staining of the distribution of HuR protein in wild-type (STHdh^{Q7/Q7}) or HD (STHdh^{Q7/Q111}) cells. The cytoplasmic/nuclear ratios of HuR signals were quantified for each cell and presented by beanplot (4 biological replicates with more than 10,000 cells for each replicate). (D) RT-qPCR quantifications of HuR-bound *HTT* mRNA levels in nuclear and cytoplasmic fractions of HD (STHdh^{Q7/Q111}) or wild-type (STHdh^{Q7/Q7}) cells detected by RNA-IP (12 technical replicates from 3 biological replicates). IgG was used as a negative control for the IP, and the 18S level was quantified as a baseline control to normalize the signals. For all plotted data, error bars represent mean and SEM. For all bean plots, the long black solid line represents the mean of each replicate, the grey dashed line represents the mean of all data points, the grey area represents the distribution of data, and short black solid lines represent the outliers of original data. The statistical analysis was performed by two-tailed unpaired t tests, *** $P < 0.001$, **** $P < 0.0001$; n.s., $P > 0.05$.

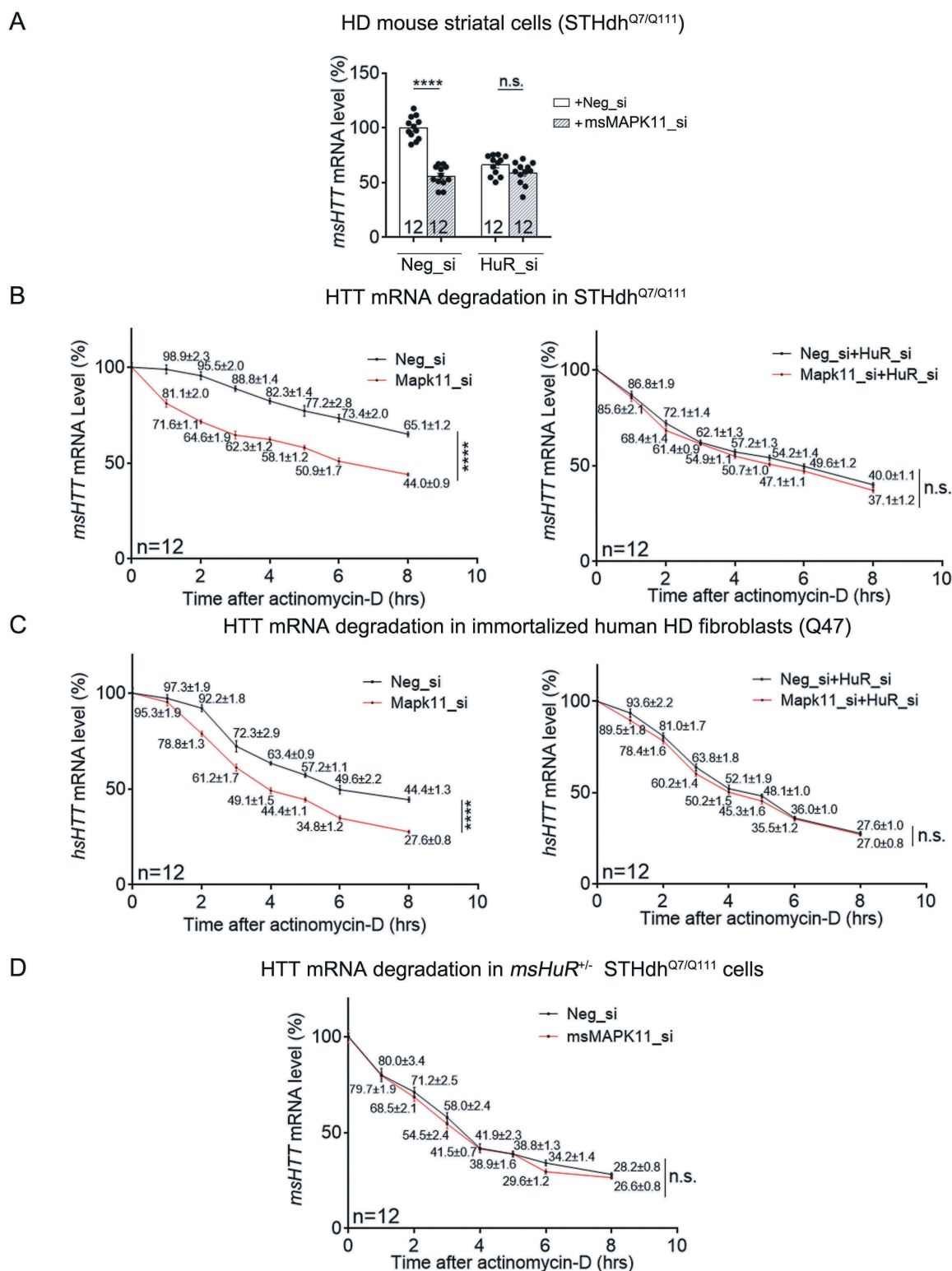


Figure 8. MAPK11 is an upstream modulator of HuR and controls HuR's regulation of *HTT* mRNA levels in HD cells.

(A) RT-qPCR quantifications of endogenous *msHTT* mRNA levels in HD mouse striatal cells (STHdh^{Q7/Q111}) transfected with the indicated siRNAs (12 technical replicates from 3 biological replicates). *msMAPK11* siRNA (grey bars) or the non-targeting control siRNA (Neg_si, white bars) were co-transfected with HuR siRNA (HuR_si) or the non-targeting control siRNA (Neg_si). *msHTT* mRNA levels were measured 48 hours after transfection. (B) *HTT* mRNA degradation measurements in HD mouse striatal cells (STHdh^{Q7/Q111}) transfected with the indicated siRNAs for 36 hours, and then treated with actinomycin D (12 technical replicates from 3 biological replicates). The quantification of *HTT* mRNA degradation was then performed the same as in Fig. 3A, B. Data values (mean ± S.E.M.) have been indicated for each point. (C) Similar to (B), but in immortalized human HD fibroblast (Q47) (12 technical replicates from 3 biological replicates). Data values (mean ± S.E.M.) have been indicated for each point. (D) Similar to (B), but in pooled colonies of mouse HD cells (STHdh^{Q7/Q111}) with the heterozygous knockout of *HuR* (12 technical replicates from 3 biological replicates). Data values (mean ± S.E.M.) have been indicated for each point. For all plotted data, error bars represent mean and SEM. The statistical analysis was performed by two-way ANOVA (B-D) or two-tailed unpaired t tests (A). *****P* < 0.0001; n.s., *P* > 0.05.

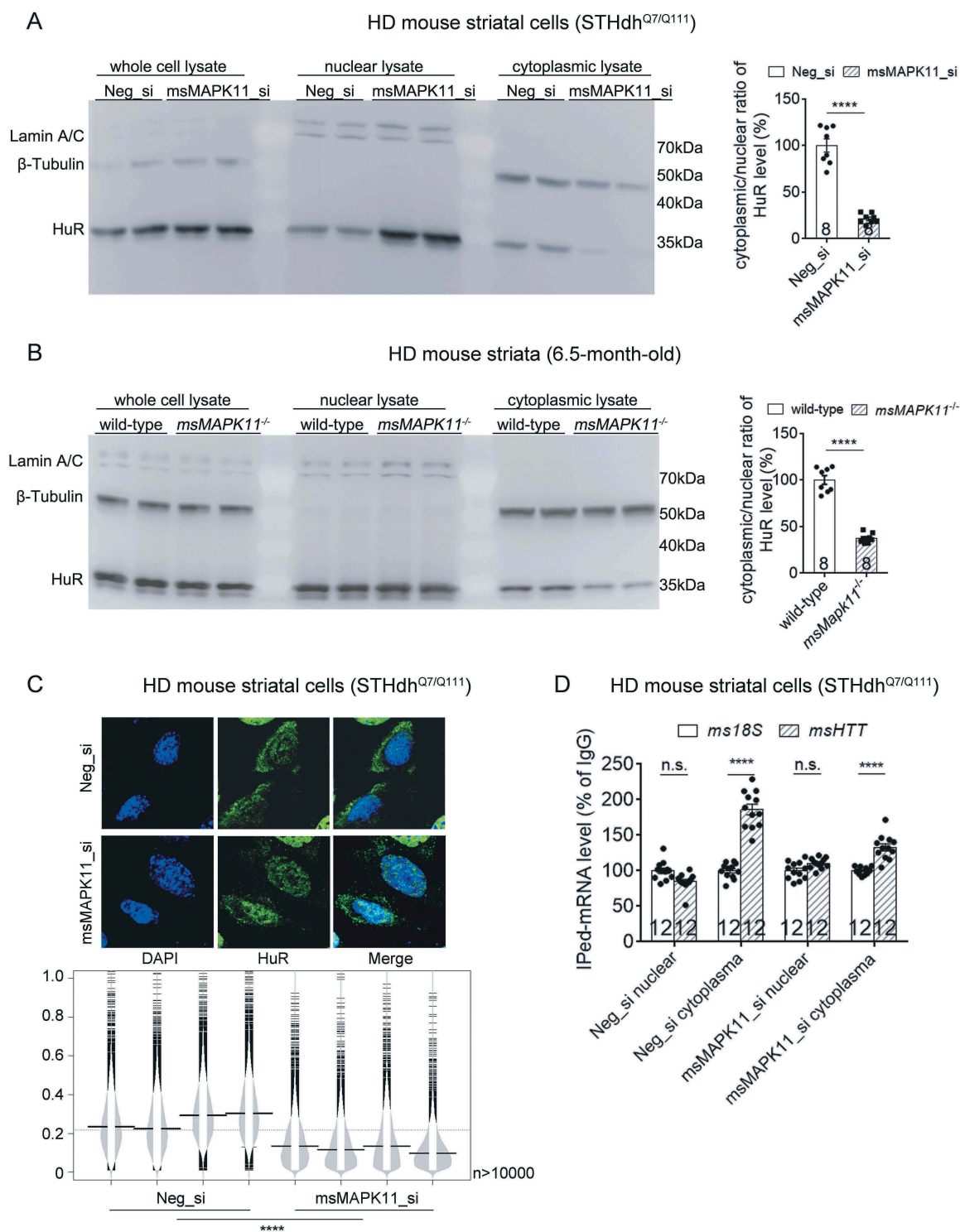


Figure 9. MAPK11 regulated nuclei/cytoplasm distribution of HuR protein in HD cells or tissues.

(A) Representative Western-blot and quantifications of cytoplasmic versus nuclear HuR protein levels in the HD mouse striatal cells (STHdh^{Q7/Q111}) transfected with the indicated siRNAs (8 technical replicates from 4 biological replicates). (B) Representative Western-blot and quantifications of cytoplasmic versus nuclear HuR protein levels in the lysates of striatal tissues from 6.5-month-old HD (*Hdh*^{Q140/Q140}) mice with or without *msMAPK11* knockout (8 technical replicates from 4 biological replicates). (C) Similar as Fig. 7C, but in HD (STHdh^{Q7/Q111}) cells transfected with the indicated siRNAs (4 biological replicates). (D) Similar as in Fig. 7D, but using HD cells transfected with the indicated siRNAs (12 technical replicates from 3 biological replicates). IgG was used as a negative control for the IP, and the 18S level was quantified as a baseline control to normalize the signals. For all plotted data, error bars represent mean and SEM. For all bean plots, the long black solid line represents the mean of each replicate, the grey dashed line represents the mean of all data points, the grey area represents the distribution of data, and short black solid lines represent the outliers of original data. The statistical analysis was performed by two-tailed unpaired t tests, ****P < 0.0001; n.s., P > 0.05.

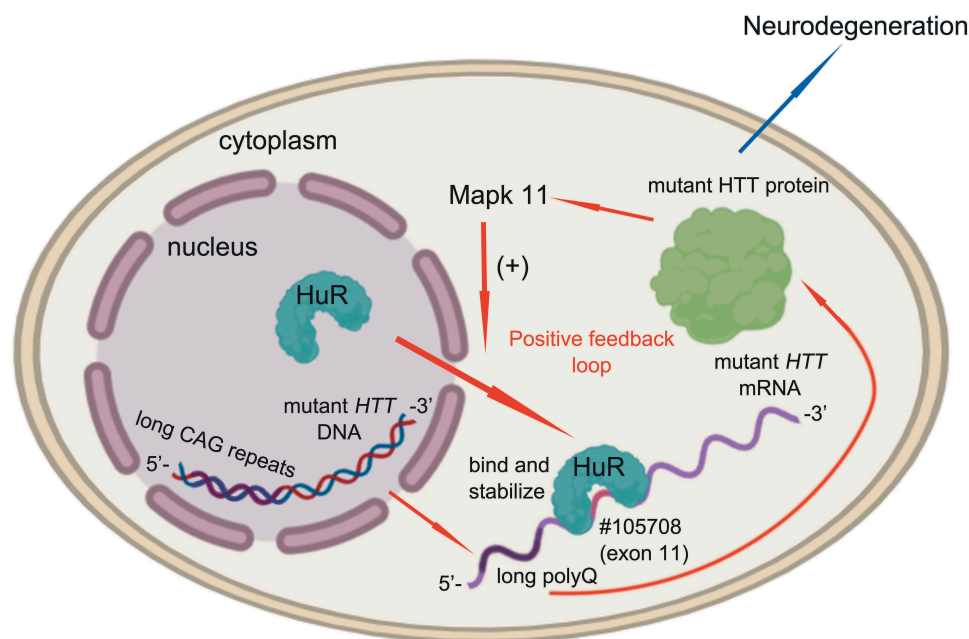


Figure 10. A schematic model illustrating mHTT-dependent MAPK11-HuR mediated regulation of *HTT* mRNA stability.

The presence of mHTT activates MAPK11 (ref. [19,20]), leading to translocation of HuR protein to the cytoplasm (ref. [21]) (Figs. 7 & 9) and its interaction with *HTT* mRNA in its exon 11 at the #105708 site (Figs. 4 & 5) to stabilize it in a mHTT-dependent manner (Figs. 2, 6 & 8B–D).

an essential protein at this stage [33,34]. Thus, HuR might play an important role at this stage through regulating wild-type HTT levels.

Material and methods

Utilization of gene symbols

The official symbol of HuR is ‘ELAVL1’, but since most of publications in the literature used ‘HuR’, we also used HuR in this paper to be consistent with others. To clarify the species, we added ‘hs’ or ‘ms’ before the gene symbol to indicate human or mouse species, respectively. In a few places where the symbol stands for both human and mouse version, ‘hs’ or ‘ms’ was not added. We used the italic font for DNAs or RNAs, and the regular font for proteins.

Plasmid constructs

The human *HTT*-exon1 (*hsHTT*exon1-Q72) and full-length (*hsHTT*-Q23 & *hsHTT*-Q73) constructs were synthesized (Thermo Fisher Scientific) and subcloned into the pcDNA/Puro-CAG plasmid vector (The schematic models of inserted constructs are shown in Fig. S4A). The human *HTT* exon 1–10 and exon 1–11 constructs were cloned by PCR amplification from the *hsHTT*-Q73 and subcloned back to pcDNA/Puro-CAG plasmid vector. All these constructs have mixed CAGCAA sequences to express the polyQ sequence. The pFRT-to-eGFP-ELAVL1 (human HuR) (Addgene, #106105) construct was obtained from Addgene. The pmirGLO Dual-Luciferase miRNA target expression vector (Promega #E1330), and all of the dual-luciferase plasmids with specific *HTT* target site (#105708, # 105717, etc.) were constructed by ligating the annealed oligos to the original backbone at the

3’UTR region of the *firefly luciferase* (Fig. S4B). The HuR-MBP.His plasmid was cloned by PCR amplification of the *HuR* cDNA from pFRT-to-eGFP-ELAVL1 plasmid and then ligated it to the pMal-c2x (Addgene, #75286; we have inserted C-terminal poly-His and the TEV protease cleavage site expressing sequence to the 3’) plasmid.

Cell culture

The patient-derived Q47 fibroblasts were described previously [19]. Human fibroblasts cell lines (GM03868 – Q45; GM21757 – Q68) and STHdh (CH00097 – Q7/Q7 and CH00096 – Q111/Q7) were obtained from Coriell Cell Repositories. HEK293T and STHdh cells were cultured in DMEM (Thermo Fisher Scientific, #11965) with 10% FBS (Thermo Fisher Scientific, #10082), whereas human fibroblasts were cultured in DMEM with 15% FBS. All the STHdh cells were maintained at 33°C incubator with 5% CO₂, and HEK293T and human fibroblasts were kept at 37°C with 5% CO₂. The cells were tested for mycoplasma contamination every month.

The homogeneous time-resolved fluorescence (HTRF) assay

The HTRF assays were performed similarly to those previously described [35]. Basically, the cells were lysed in the lysis buffer (1× PBS with 0.4% Triton X-100 and 1× protease inhibitor final) and the *HTT* protein was detected with 2B7/MW1 antibody pair. For all samples, the total protein concentration (by BCA, Beyotime, #P0009) was measured to correct the loadings. Different protein concentrations or cell numbers per well were tested to ensure that the signals were

in the linear range. Background corrections were performed by subtracting the background signals from blank samples.

cDNA and siRNA transfection

All cDNAs were transfected with lipofectamine 3000 (Life Technologies, # L3000), whereas siRNAs were transfected into the STHdh cells with lipofectamine 2000 (Life Technologies, #11668). Transfection steps were performed according to the manufacturer's protocol. Cells were collected at different timelines for diverse experimental purpose. Briefly, cells were collected 24 hours after plasmid transfection for dual-luciferase detection, or 48 hours after cDNA or siRNA transfection for qPCR or RNA-IP, or 72 hours after siRNA transfection for Western blot or HTRF. In some experiments (Figs. 2E, 4D & 5D), the cells were first transfected with siRNA and then with cDNA. In this case, the siRNA was first transfected for 24 hours. The culture medium was then changed, and the cDNA transfection was performed. The cells were then collected for experiments 48 hours after cDNA transfection. All siRNAs have been validated by qPCR and/or western blots for target knockdown. siRNA target sequences are shown as below: HuR_siRNA 1 (both human and mouse): AAGAGGCAATTACCAGTTTCA; HuR_siRNA 2 (both human and mouse): GGGATAAAGTAGCAGGACA; MAPK 11_siRNA (human): CACGCATGTATGCATGC ACAA; Mapk 11_siRNA (mouse): CGCCAGAGATCATGC TAAA. Neg_siRNA was purchased commercially (QIAGEN, #1027280).

RT-qPCR and mRNA stability measurements

mRNA levels were determined by RT-qPCR, and the protocol was followed as previously described. Briefly, RNA from siRNA-transfected and/or actinomycin D-treated cells was extracted using RNAPrep Pure Cell/Bacteria Kit according to the manufactory's instruction (Tiangen, #DP430). cDNA was obtained by reverse transcription with random primers using the FastQuant RT Kit (Tiangen, #KR106). qPCR was then performed using SYBR Green Realtime PCR Master Mix (Toyobo, #QPK-201) with no reverse-transcriptase controls used to ensure the specificity of the signals. All the primers were tested with a standard curve (Fig. S5).

For mRNA stability measurements, the cultured cells were treated with actinomycin D (5 µg/ml, Sigma, #A9315) that inhibits transcription at time 0, and then collected at indicated time points for quantification of different mRNAs by RT-qPCR. The qPCR primer sequences are (note that STHdh^{Q7/Q111} cells express the mouse wild-type *HTT* mRNA, as well as a mouse-human chimera *HTT* mRNA with its exon1 and part of intron 1 replaced by the human version with expanded CAG repeats (111 CAG), but the *msHTT* qPCR primers targeting the 3' sequences can detect both): *hs18S*-forward: GGTGGAGCGATTTGTCT GGTTA; *hs18S*-reverse (human): CGGACATCTAAGGG CATCACAG; *ms18S* -forward (mouse): CGCCGCTAGAGGT GAAATC; *ms18S*-reverse (mouse): CCAGTCGGCATCGTT TATGG; *hsHTT*-forward: CCTTTTGAAGCAGCCCGTG; *hs HTT*-reverse: TGCAGCATCCCCAACAGAT; *msHTT*-forward (mouse): GCAGAGATTTGGCTGCATTC; *msHTT*-

T-reverse (mouse): CCATGGCATAACAGCAGCA; *hsHuR*-forward (human): GGCTTGAGGCTCCAGTCAAA; *hsHuR*-Reverse (human): CCCTCTGGACAAACCTGTAGT; *msHuR*-forward (mouse): CACCACCAGGCACAGAGATT; *msHuR*-reverse (mouse): CGGGGACATTGACACCAGAA; *EGFP*-forward: TATATCATGGCCGACAAGCA; *EGFP*-reverse: GTTGTGGCGGATCTTGAAGT; exon 1–11 of mutant *HTT*-forward: CACCGCTGCTAAGGAGGA; exon 1–11 of mutant *HTT*-reverse: AGGAACCCCTCCAGCTA; *hsHTT* exon 1-Q72-forward: CCTCAGCCACAACCTCCTC; *hsHTT* exon 1-Q72-reverse: CGTATGGGTATCGGTGCAG

RNA immunoprecipitation (RNA-IP)

To perform RNA-IP, protein G magnetic beads (Bio-rad, #161-4023) were first blocked with 5% BSA and 2 µg/mL tRNA on a roller for 1.5 hours at 4 °C. Then mixed the beads with antibody in RIP buffer (100 mM KCl + 25 mM Tris-HCl (pH = 7.4) + 1 mM EDTA + 0.5 mM DTT + 0.5% NP-40 + 1× RNase inhibitor (Thermo Fisher Scientific, #N8080119) + 1× Complete protease inhibitor (Roche, #04693132001)) overnight on a roller at 4 °C. The next day, cell samples were collected and lysed by the RIP buffer, and one-third of the sample was kept as the input control before pull-down by the antibody-conjugated beads. The lysates were incubated with the beads overnight on a roller at 4 °C, and then the beads were washed by cold RIP Buffer followed by 1× PBS once. The RNA pulled down by the beads was then isolated by RNA simple Total RNA kit (TIANGEN, #DP419). The mRNA level was then measured and analysed by RT-qPCR, as illustrated above.

RNA electrophoretic mobility shift assay (R-EMSA)

The human HuR protein was purified for the R-EMSA experiments. To obtain the recombinant purified HuR protein, HEK293T cells were transfected with the HuR-MBP.His plasmid, and then collected after 48h. The cellular protein was then extracted by NiA Buffer (20 mM imidazole + 5% glycerol + 150 mM NaCl + 100 mM Tris-HCl (pH = 7.4) + 1 × Complete protease inhibitor (Roche, #04693132001)), and then loaded onto the Ni-NTA superflow column (QIAGEN, #30622). Column bound proteins were then eluted by NiB Buffer (300 mM imidazole + 5% glycerol + 150 mM NaCl + 100 mM Tris-HCl (pH = 7.4) + 1 × Complete protease inhibitor (Roche, #04693132001)). Finally, the purified proteins were concentrated to approximately 2 mg/ml in 50 mM HEPES buffer with 100 mM NaCl for further analysis, and the purity of HuR protein was confirmed by coomassie brilliant blue staining. To perform RNA-EMSA, the Cy3-labelled RNA oligos (4µM) were first heated to 95 °C and cooled down to 25 °C at room temperature. Then the titrated HuR protein (2 mg/mL) and RNA oligos were dissolved in the EMSA interaction buffer (1 × R-EMSA Binding Buffer (Thermo Fisher Scientific, #20158) + 5% glycerol + 100 µg/mL tRNA+1× RNase inhibitor (Thermo Fisher Scientific, #N8080119)), and then incubated for 30 min at room temperature (25 °C). The reaction mixture was then loaded onto a 6% acrylamide native gel and run the electrophoresis at 4 °C. Shift band intensities were captured by Typhoon FLA-9000 (GE).

Nuclear/cytoplasmic protein extraction and Western-blots

The nuclear/cytoplasmic protein extraction was performed in the same way as previous reports [36]. Cell pellets were collected and lysed on ice for 5 min in lysis buffer (50 mM Tris-HCl (pH = 7.4) + 10 mM NaCl + 0.5% NP-40 + 0.25% Triton X-100 + 1 mM EDTA + 1× Complete protease inhibitor (Roche, #04693132001)) and centrifuged at 3000 × g at 4 °C for 5 min. The nuclear compartments were in the precipitates, and the supernatants then contained cytoplasmic proteins. Then the precipitates were washed with the lysis buffer once and resuspended in the NET Buffer (20 mM HEPES + 1.5 mM MgCl₂ + 0.5 M NaCl + 0.2 mM EDTA + 20% glycerol + 1% Triton X-100), sonicated for 0.8 minutes at 17 W, and then centrifuged at 10000 × g at 4 °C for 10 min. The supernatants collected at this time then contains specific proteins from the nuclei. Western-blots for the nuclei marker Lamin A/C and cytoplasmic marker β-Tubulin were performed to confirm the nuclei/cytoplasm separation (Figs. 7A, B, & 9A, B). For whole cell lysates, 10⁶ cells were collected and resuspended in 100 μl PBS-Triton X Buffer (1 × PBS + 1% Triton X-100) with 1× Complete protease inhibitor (Roche, #04693132001) on ice for 30 min. The suspension was sonicated for 0.8 minutes at 17 W and then centrifuged at 20000 × g at 4 °C for 10 min. The supernatant was kept as the total cell protein. All the protein samples were then loaded and transferred onto nitrocellulose membranes for Western-blots. Commercially purchased antibodies include anti-HuR (Proteintech, #11910-1-AP), anti-β-Tubulin (Abcam, #ab6046), anti-Lamin A/C (Proteintech, #10298-1-AP), anti-p38-β2 (Invitrogen, #33-8700). The specificity of all antibodies has been validated by previous reports or our knockdown or knockout experiments.

Immunofluorescence and high-content imaging

For immunofluorescence, cultured cells were washed three times with 1× PBS and then fixed in 4% paraformaldehyde (PFA) for 15 minutes, followed by permeablizing in 0.5% TritonX-100 for 10 min. The cells were then blocked in 4% BSA + 0.1% Triton X-100 in 1× PBS and incubated with primary antibodies at 4°C overnight, and then washed with blocking buffer and incubated with secondary antibody at room temperature for 1 h. The samples were then washed, 0.5 mg/ml DAPI (Beyotime Biotechnology, #C1002) was added for 5 min before the cells were final washed and stored in 1× PBS. The images of samples were scanned and then analysed by the high-content imaging system Operetta CLS (PerkinElmer) and its accompanying software Harmony 4.8. The bean plots of the analysed data were generated by online application: <http://shiny.chemgrid.org/boxplotr>, which was developed according to the description of Nature Method [37].

Statistical analysis

Statistical comparisons between two groups were conducted by the two-tailed unpaired Student's t-tests. Statistical comparisons among multiple groups were conducted by ANOVA tests.

Significance was established at P < 0.05. In all graphs, error bars indicate SEM, and the biological replicate numbers are indicated on top of each bar and/or as the n numbers in the legends. The statistical powers for all analysis were calculated and confirmed to be > 80%. Data were excluded when there were clear indications of the artefact or experimental failures, such as contamination, transfection/infection failure, etc.

Acknowledgments

We would like to thank Dr. Yang Li for kindly providing the pmirGLO plasmids. We would like to thank Drs. Jianhua Gan and Binglian Zheng for providing insightful discussion and technical supports.

Data availability

The CLIP-seq data analysis results were obtained from the previously published database StarBase, which is available at: <http://starbase.sysu.edu.cn/>;

The RBP expression was analyzed by the BioGPS database, which is available at: <http://biogps.org/#goto=welcom>

The accession numbers of the genes relevant to this study include:

HTT-huntingtin [*Homo sapiens*] (*hsHTT*): Gene ID 3064

Htt-huntingtin [*Mus musculus*] (*msHTT*): Gene ID 15194

ELAVL1-HuR [*Homo sapiens*] (*hsHuR*): Gene ID 1994

Elavl1-HuR [*Mus musculus*] (*msHuR*): Gene ID 15568

MAPK11 [*Homo sapiens*] (*hsMAPK11*): Gene ID 5600

Mapk11 [*Mus musculus*] (*msMAPK11*): Gene ID 19094

All the gene information is available at: <https://www.ncbi.nlm.nih.gov/gene>

Disclosure statement

No potential conflict of interest was reported by the authors.

Funding

Project Supported by National Natural Science Foundation of China [31970747, 31601105, 81870990, 81925012], Science and Technology Commission of Shanghai Municipality [18410722100], Shanghai Municipal Science and Technology Major Project [No.2018SHZDZX01] and ZJLab, and Hereditary Disease Foundation for funding supports. Funding for open access charge: National Natural Science Foundation of China.

ORCID

Jian Wang  <http://orcid.org/0000-0002-2748-395X>

Boxun Lu  <http://orcid.org/0000-0002-1675-9340>

References

- [1] TheHuntington'sDiseaseCollaborativeResearchGroup. A novel gene containing a trinucleotide repeat that is expanded and unstable on Huntington's disease chromosomes. *Cell*. 1993;72:971–983.
- [2] Rubinsztein DC, Carmichael J. Huntington's disease: molecular basis of neurodegeneration. *Expert Rev Mol Med*. 2003;5:1–21.
- [3] Feng X, Luo S, Lu B. Conformation polymorphism of polyglutamine proteins. *Trends Biochem Sci*. 2018;43:424–435.
- [4] Rodriguez-Lebron E, Denovan-Wright EM, Nash K, et al. Intrastriatal rAAV-mediated delivery of anti-huntingtin shRNAs induces partial reversal of disease progression in R6/1 Huntington's disease transgenic mice. *Mol Ther*. 2005;12:618–633.

- [5] Harper SQ, Staber PD, He X, et al. RNA interference improves motor and neuropathological abnormalities in a Huntington's disease mouse model. *Proc Natl Acad Sci U S A*. 2005;102:5820–5825.
- [6] DiFiglia M, Sena-Esteves M, Chase K, et al. Therapeutic silencing of mutant huntingtin with siRNA attenuates striatal and cortical neuropathology and behavioral deficits. *Proc Natl Acad Sci U S A*. 2007;104:17204–17209.
- [7] Kordasiewicz HB, Stanek LM, Wancewicz EV, et al. Sustained therapeutic reversal of Huntington's disease by transient repression of huntingtin synthesis. *Neuron*. 2012;74:1031–1044.
- [8] Tabrizi SJ, Leavitt BR, Landwehrmeyer GB, et al. Targeting Huntingtin expression in patients with Huntington's disease. *N Engl J Med*. 2019;380:2307–2316.
- [9] Chung DW, Rudnicki DD, Yu L, et al. A natural antisense transcript at the Huntington's disease repeat locus regulates HTT expression. *Hum Mol Genet*. 2011;20:3467–3477.
- [10] Ito D, Hatano M, Suzuki N. RNA binding proteins and the pathological cascade in ALS/FTD neurodegeneration. *Sci Transl Med*. 2017;9:eaah5436.
- [11] Yu S, Liang Y, Palacino J, et al. Drugging unconventional targets: insights from Huntington's disease. *Trends Pharmacol Sci*. 2014;35:53–62.
- [12] Li JH, Liu S, Zhou H, et al. starBase v2.0: decoding miRNA-ceRNA, miRNA-ncRNA and protein-RNA interaction networks from large-scale CLIP-Seq data. *Nucleic Acids Res*. 2014;42:D92–97.
- [13] Wu C, Jin X, Tsung G, et al. BioGPS: building your own mash-up of gene annotations and expression profiles. *Nucleic Acids Res*. 2016;44:D313–316.
- [14] Trettel F, Rigamonti D, Hilditch-Maguire P, et al. Dominant phenotypes produced by the HD mutation in STHdh(Q111) striatal cells. *Hum Mol Genet*. 2000;9:2799–2809.
- [15] Peng SS, Chen CY, Xu N, et al. RNA stabilization by the AU-rich element binding protein, HuR, an ELAV protein. *Embo J*. 1998;17:3461–3470.
- [16] Ke Y, Han Y, Guo X, et al. PARP1 promotes gene expression at the post-transcriptional level by modulating the RNA-binding protein HuR. *Nat Commun*. 2017;8:14632.
- [17] Fan XC, Steitz JA. Overexpression of HuR, a nuclear-cytoplasmic shuttling protein, increases the in vivo stability of ARE-containing mRNAs. *Embo J*. 1998;17:3448–3460.
- [18] Fan XC, Steitz JA. HNS, a nuclear-cytoplasmic shuttling sequence in HuR. *Proc Natl Acad Sci U S A*. 1998;95:15293–15298.
- [19] Yu M, Fu Y, Liang Y, et al. Suppression of MAPK11 or HIPK3 reduces mutant Huntingtin levels in Huntington's disease models. *Cell Res*. 2017;27:1441–1465.
- [20] Taylor DM, Moser R, Regulier E, et al. MAP kinase phosphatase 1 (MKP-1/DUSP1) is neuroprotective in Huntington's disease via additive effects of JNK and p38 inhibition. *J Neurosci*. 2013;33:2313–2325.
- [21] Joassard OR, Belanger G, Karmouch J, et al. HuR mediates changes in the stability of AChR beta-subunit mRNAs after skeletal muscle denervation. *J Neurosci*. 2015;35:10949–10962.
- [22] Xiao L, Li X, Chung HK, et al. RNA-binding protein HuR regulates paneth cell function by altering membrane localization of TLR2 via posttranscriptional control of CNPY3. *Gastroenterology*. 2019;157:731–743.
- [23] Jain A, Vale RD. RNA phase transitions in repeat expansion disorders. *Nature*. 2017;546:243–247.
- [24] Swami M, Hendricks AE, Gillis T, et al. Somatic expansion of the Huntington's disease CAG repeat in the brain is associated with an earlier age of disease onset. *Hum Mol Genet*. 2009;18:3039–3047.
- [25] Tabrizi SJ, Ghosh R, Leavitt BR. Huntingtin lowering strategies for disease modification in Huntington's disease. *Neuron*. 2019;102:899.
- [26] Genetic Modifiers of Huntington's Disease Consortium. Electronic address, g.h.m.h.e. and Genetic Modifiers of Huntington's Disease, C. CAG repeat not polyglutamine length determines timing of Huntington's disease onset. *Cell*. 2019;178:887–900 e814.
- [27] Frantz B, Klatt T, Pang M, et al. The activation state of p38 mitogen-activated protein kinase determines the efficiency of ATP competition for pyridinylimidazole inhibitor binding. *Biochemistry*. 1998;37:13846–13853.
- [28] Lang M, Berry D, Passecker K, et al. HuR small-molecule inhibitor elicits differential effects in adenomatous polyposis and colorectal carcinogenesis. *Cancer Res*. 2017;77:2424–2438.
- [29] Saudou F, Humbert S. The biology of Huntingtin. *Neuron*. 2016;89:910–926.
- [30] Kim EK, Choi EJ. Compromised MAPK signaling in human diseases: an update. *Arch Toxicol*. 2015;89:867–882.
- [31] Buren C, Wang L, Smith-Dijak A, et al. Region-specific pro-survival signaling and global neuronal protection by wild-type Huntingtin. *J Huntingtons Dis*. 2014;3:365–376.
- [32] Bradham C, McClay DR. p38 MAPK in development and cancer. *Cell Cycle*. 2006;5:824–828.
- [33] Zeitlin S, Liu JP, Chapman DL, et al. Increased apoptosis and early embryonic lethality in mice nullizygous for the Huntington's disease gene homologue. *Nat Genet*. 1995;11:155–163.
- [34] Nasir J, Floresco SB, O'Kusky JR, et al. Targeted disruption of the Huntington's disease gene results in embryonic lethality and behavioral and morphological changes in heterozygotes. *Cell*. 1995;81:811–823.
- [35] Lu B, Al-Ramahi I, Valencia A, et al. Identification of NUB1 as a suppressor of mutant Huntington toxicity via enhanced protein clearance. *Nat Neurosci*. 2013;16:562–570.
- [36] Tollervey JR, Curk T, Rogelj B, et al. Characterizing the RNA targets and position-dependent splicing regulation by TDP-43. *Nat Neurosci*. 2011;14:452–458.
- [37] Spitzer M, Wildenhain J, Rappsilber J, Tyers M. Boxplotr: a web tool for generation of box plots. *Nature Methods*. 2014;11:121–122. DOI: [10.1038/nmeth.2811](https://doi.org/10.1038/nmeth.2811)